

**Introduction:** Mars Global Surveyor (MGS) measured the most strongly magnetized crust in the heavily-cratered southern hemisphere of Mars, with the magnetic intensity reaching nearly 10 times that of Earth's magnetic lineations. We concentrate our analysis on the magnetic lineations or patterns centered near latitude  $40^{\circ}\text{S}$ , longitude  $180^{\circ}\text{W}$ , with a range of values  $\pm 40^{\circ}$ , using a rotated Cartesian coordinate system. The data utilized was from the mapping phase of MGS, MAG/ER magnetic measurements at altitudes of  $404 \pm 30$  km (made available by Connerney and coauthors, conveniently averaged, sorted and binned into 180 latitude and 360 longitude bins by degree, providing estimates of each component in a spherical coordinate system with  $r$ , radial,  $\phi$  (east-west) and  $\theta$  (north-south) components [1].

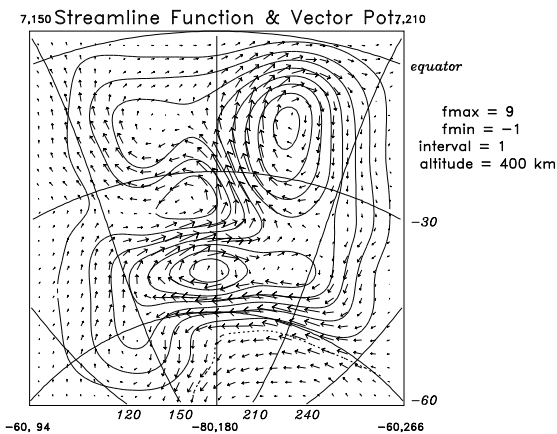


Figure 1: The streamline function and vector potential at 400 km, satellite mapping level. Map centered at  $40^{\circ}\text{S}, 180^{\circ}\text{W} \pm 40^{\circ}$ , extending  $40^{\circ}$  in each direction. Latitude and longitude lines, with the geographical coordinates of the corners given.

We consider the subset of data within  $\pm 40^{\circ}$  of  $40^{\circ}\text{S}$  and  $180^{\circ}$ , i.e. longitudes  $140^{\circ}$  to  $220^{\circ}$ , latitudes  $0^{\circ}$  to  $-80^{\circ}$ . We then convert these latitudes and longitudes to Cartesian coordinates and use an ordinary two-dimensional Fourier analysis for downward continuation. This can be shown to be a good approximation: results can be used to reconstruct the original components as a check on the coordinate transformation [2]. Also, we show [2] that the downward continuation of the MGS mapping-phase data at 400 km very closely matches the measurements at 100 km made during the aerobraking phase [3], filling in the data gaps. The advantage of this coordinate system is the lack of distortion; it extends 40 degrees in each direction about the center.

This region,  $40^{\circ}\text{S} \pm 40^{\circ}, 180^{\circ}\text{W} \pm 40^{\circ}$ , covers nearly an octant of the planet and encompasses the most strongly magnetized crust on Mars. Our goal is to describe the magnetic

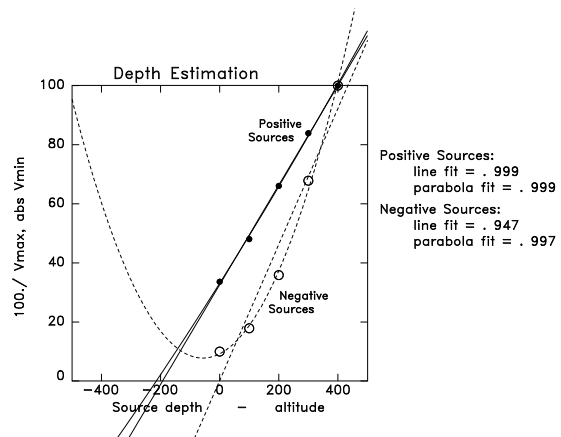


Figure 2: Comparison of maximum and minimum values of streamline function at depths from 400 km to surface.

field by means of a vector potential which is the curl of a streamline function because they are simpler, smoother and more fundamental than working with the three components of the magnetic field. The magnetic field components can be described by the curl of the vector potential. The streamline function can be modeled simply, and the other components can be derived from it.

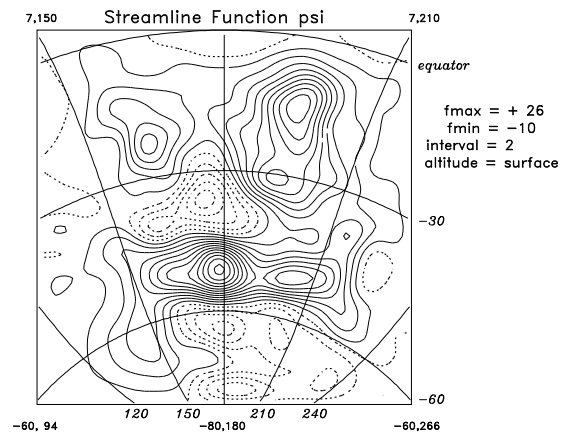


Figure 3: The streamline function obtained from the vertical component of the magnetic field using a Fourier transform and extrapolated downwards from 400 to the surface. Map projection as in Fig. 1

**Analysis:** The streamline function is constructed from the vertical component of the magnetic field, taking the Fourier transform and dividing by the vertical wavenumber squared,

then inverse transforming [4]. This function shown in Fig. 1 has also been extrapolated to the surface. As can be seen, the streamline function at satellite level is decidedly skewed and the vector potential field swirls around only in one direction. Does this suggest lack of reversals? The vector potential, though more challenging to present, is intuitive in the sense that it represents the field as a swirl around an axis. The vector potential (Fig. 1) shows abrupt changes in direction which suggest different ages of magnetization or demagnetization for adjacent regions. Finally, the vector potential enters directly in Shroedinger's equation and would cause energy and angular momentum transitions and so magnetic realignments for capturing a thermal event.

**Models:** As we extrapolate downward from 400 km to the surface using Laplace's equation, the minimum and maximum values increase rapidly. If we plot their reciprocals against the altitude (Fig. 2), we see that the fields cannot be extrapolated far below the surface. This reveals a systematic difference in the behavior of the positive (solid circles) and negative sources (open circles) as they are extrapolated downwards.

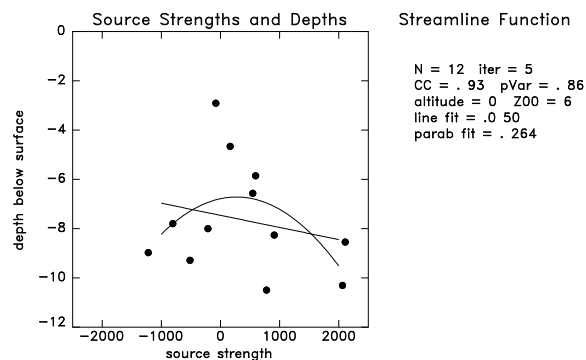


Figure 4: Source strengths and depths obtained by fitting vertical dipoles to 12 centers. The model accounts for 86% of the variance with a 0.93 correlation coefficient.

We model the magnetic field using the observed streamline function at the surface (Fig. 3). With vertical dipoles we determine depths and magnitudes for selected centers and average surroundings, and find that at the surface that 12 sources account for >80% of the variance. (Only 4 sources already account for >60% of the variance.) These sources range in depth  $260 \pm 130$  km, but the source magnitudes range over a factor of 4. Figure 4 shows a scatter diagram of the source magnitudes and the depths for this model. Generally, the smaller sources are shallower, and the larger sources tend to be deeper. However, this relationship is described by a parabolic fit only accounts for about 1/4 of the variance, but better than a linear fit. There also exists an obvious asymmetry in the relative proportion of the positive and negative sources, and their depth

versus strength.

Major questions about the origin and nature of Mars' magnetism remain. Initially, the magnetization were interpreted as lineations with reversals [1] that could indicate a process like Earth's seafloor spreading on Mars. However, other interpretations can be made. Cain et al. constructed a 90 degree and order global spherical harmonic model of the scalar potential, cautioning that the choices for contouring and color strongly influence visual appearance and interpretation of magnetic patterns [5]. Our model for the scalar potential [2] and streamline function (Fig. 3) depicts small regions with intense magnetization. Also, in a planetary model fitted to aerobraking data, the strong magnetization in the southern hemisphere has been interpreted in terms of equidimensional sources rather than lineations [6].

The streamline function, extrapolated to the planet's surface from satellite level can be compared with surface features (Fig. 3). Highland terrain materials with some younger northern channel materials and southern polar deposits cover the region analyzed [7,8,9]. Of particular interest are the location of ancient impacts that no longer retain the topographic signature of fresh craters, but instead are identified by concentric basins and outflow channels [10]. Generally, impact craters larger than 300 km disrupt magnetization [3] even out to several radii. However, in the southern hemisphere modification of the surface magnetization is not obvious. Indeed, some of the strongest streamline function lies adjacent to the rings of the ancient impacts. Possibly, then, in the southern hemisphere magnetization followed the early impacts causing the large basins like Sirenum.

**Conclusion:** The magnetic vector potential, while more difficult to display, is more fundamental than the scalar potential, and suggests a much simpler interpretation of magnetic patterns in the region near  $40^\circ\text{S}, 180^\circ\text{W} \pm 40^\circ$ . This region encompasses the most strongly magnetized area concentrated in the older, more heavily cratered Southern hemisphere, and shows no disruption due to ancient craters. The patterns of magnetization in this region are shown to be more equidimensional than linear. In addition, modeling of the field shows the source distribution to be skewed, with few and weaker negative sources than positive ones, and deeper locations for the larger sources.

**References:** [1] Connerney, J.E.P. et al. (2001), *GRL*, 28, 4015-4018. [2] Jurdy, D.M. and M. Stefanick (2004), *JGR*, 109, 10.1029/2004JE002277. [3] Acuna M.H. et al. (1999), *Science*, 284, 790-793. [4] Blakely, R.J. (1996), *Potential theory in gravity and magnetic applications*, Cambridge Univ. Press, 441pp. [5] Cain, J.C., et al. (2003), *JGR*, 108, 5008. [6] Arkani-Hamed, J. (2001), *JGR* 106, 23197. [7] Greely, R., and J.E. Guest (1987), USGS, Geologic map of the eastern equatorial region of Mars.. [8] Scott, D.H., and Tanaka, K.L. (1986), USGS, Geologic map of the western equatorial region of Mars. [9] Tanaka, K.L., and Scott, D.H. (1987), USGS, Geologic map of the polar regions of Mars. [10] Schultz, P.H. et al. (1982), *JGR* 8, 9803.